Antal Kerpely Doctoral School of Materials Science and Technology

Foam glass production and characterization based on waste materials: container glass, cathode ray tube glass, and aluminium dross

Thesis Booklet

By

Meriem Sassi

Supervisor

Dr. Andrea Simon, Associate Professor

Head of the Doctoral School

Prof. Dr. Valéria Mertinger

Institute of Ceramic and Polymer Engineering

Faculty of Materials and Chemical Engineering

University of Miskolc

Miskolc, Hungary

2023

1. Introduction

Foam glass is a lightweight insulating material with high chemical stability whose density and texture may vary depending on its initial chemical composition. It was invented in 1931s, by sintering silica with combustible material (lignite, coal, wood), and foaming agents (hydrochloric acid, sodium hydroxide) at 1500°C. Foam glass was granted many patents at once, causing uncertainty as to who invented it first [1]. Foam glass is essentially made of powder glass and foaming agent, mixed and heated above the softening point of the glass. Then, the foaming agent decomposes and releases gaseous products, driving the expansion of the glass [8] [9]. Researchers employed a variety of foaming agents and stabilizers to create foams with the best insulation properties. Commercial foam glass has a low density (120-160 kg/m^3), a compressive strength ranging between 0.6 to 1.0 MPa, a high thermal resistance (0.04-0.07 W/m·K), and a low water absorption ($\leq$ 5-6 kg/m^2 after 28 days) [5] [6] [7].

Currently, the focus is diverted to producing Eco-friendly foams based on waste materials to decrease the depletion of natural resources and the costs of the raw materials as consequences the unit price of the commercial foam glass. This research aims to create foam glass from 100% waste material, including two types of hazardous waste. By reducing production costs and increasing insulation capacity, we aim to produce affordable and reliable insulating materials without compromising the environment.

1.1. Summary of the literature

Foam glass is primarily composed of up to 98% glass powder. In its original formulation, virgin glass was the only material used to create glass foam. The initial particle size, the composition of the raw materials, and the sintering temperature and rate can affect the properties of the foam glass. As of now, several foam glass production plants are using up to 98 wt% post-consumer glass waste [15]. Different materials can be introduced in the production of foam glass mainly fly ash, $CaCO_3$[17], windowpanes wastes [20], high titanium blast furnace slag [21], used mineral wool waste [25] [26], metakaolin [27], fayalite slag [30], lead-zinc mine tailings, red mud [32], polymetallic ore tailings [33] and, coal gangue [36].

One of the materials that can be used in foam glass production is cathode-ray tube glass (CRT). CRT glass comes from computer monitors and TV sets. The replacement of cathode ray tube screens with flat panels increased the electronic waste [40] [41]. CRT glass usually contains phosphor, cadmium, lead, and other metals (strontium, antimony, barium, europium, selenium, etc.). Lead can cause the risk of dispersing poisonous substances during remelting making CRT recycling difficult [42]. CRT glass can be directly used as a secondary raw material without considering the lead content in building materials (glass-ceramic bricks and concrete materials), glass base materials, radiation protection materials, and low-cost adsorbent materials [40]. On the other hand, lead can be extracted and treated by three methods: pyrometallurgy, hydrometallurgy [45], and mechanical activation [40].

Another material that can be used in foam glass production is aluminium dross. It is a non-biodegradable waste produced by the secondary aluminium industry during aluminium scrap [64]. The global aluminium dross generation is more than four million tons per year [61]. Aluminium dross composition varies depending upon the operation of the plants. Usually, dross contains 15-30 wt% aluminium oxide, 30-55 wt % sodium chloride, 15-30 wt % potassium chloride, 5–7 wt % metallic aluminium, and impurities (carbides, nitrides, sulphides, and phosphides) [58] [59]. In contact with water or even air humidity these impurities can generate toxic, harmful, explosive, and unpleasant odorous gases, such as NH_3, CH_4, PH_3, H_2, H_2S. It is classified as hazardous waste that is prohibited to landfill in most of the European countries [60]. One alternative way of recycling dross is to use it directly in the generation of valuable products: as an additive for the synthesis of composites, alloys, derivative compounds of aluminium, aluminium-alumina refractories, refractory coatings[5], glass ceramics [73] [74] [69] [75], geopolymer [64], as a clay replacement in lightweight aggregate [76], cement clinker

production [64], as a partial replacement for sand in sandcrete blocks [60], and as a catalyst support for glycerol dry reforming [77].
Because of the hazardous characteristics of those materials, the hydrolytic and chemical stability of the final product should be studied. At the same time foam glass should be resistant to all kinds of liquid and vapor chemicals to ensure long-term performance [86].

1.2.Research gap

The main object of this research is to produce foam glass with 100% waste materials (container and CRT glasses and aluminium dross) with optimal chemical and physical properties and long-life span. The major rising questions are:

- How to evaluate and control the foaming process?
- Which particle size of the raw materials will give the optimal properties?
- What is the effect of adding CRT glass to foam glass?
- What is the effect of adding different type of aluminium dross?
- What is the porosity type of the resultant foam glass?
- Do the hazardous elements remain stable in the foam glass? does the final product compile with the European regulations?
- What is the predicted life span of the final product?

2. Materials and Methods

2.1.Raw materials and samples preparation

Raw materials were prepared to produce foam glass (Figure 1). Container glass was collected, cleaned, crushed, and milled. The particle size of the glass powder was determined using a Horiba Laser Scattering Particle Size Distribution Analyzer LA-950. The powder was sieved with a 63 μm sieve. Two particle size of the CRT glass was provided (63 and 32 μm) by Daniella Ipari Park Ltd. Aluminium drosses (64, X, 53) with different composition were used (produced by Arconic-Köfém Mill Products Hungary Ltd., Szekesfehervar, Hungary). The metal and salt content of the as-received dross was removed by Kekesi et al. [92]. In the mixtures, container glass was the basic component. CRT glass was added in 5 and 10 wt%. Firstly, I added 10, 20, and 30 wt% dross then I adjusted the amount to 10, 15 or 20 wt% dross. In all the samples, 2 wt% silicon carbide was admixed as a foaming agent (α-SiC with particle size less than 32 μm). From each composition, 100 g was prepared and homogenized. Five grams from each mixture were poured in a stainless-steel mold then pressed under 11 MPa for 10 s into a cylindrical shape (diameter = 20 mm, height = 11 mm) and 20 samples from each mixture were prepared. To determine the exact foaming temperature for sintering, a heating microscope (MicrOvis, Camar Elettronica) were used. The samples were sintered in an electric chamber furnace at different temperatures with a heating rate of 5 °C/min and a holding time of 10 min.

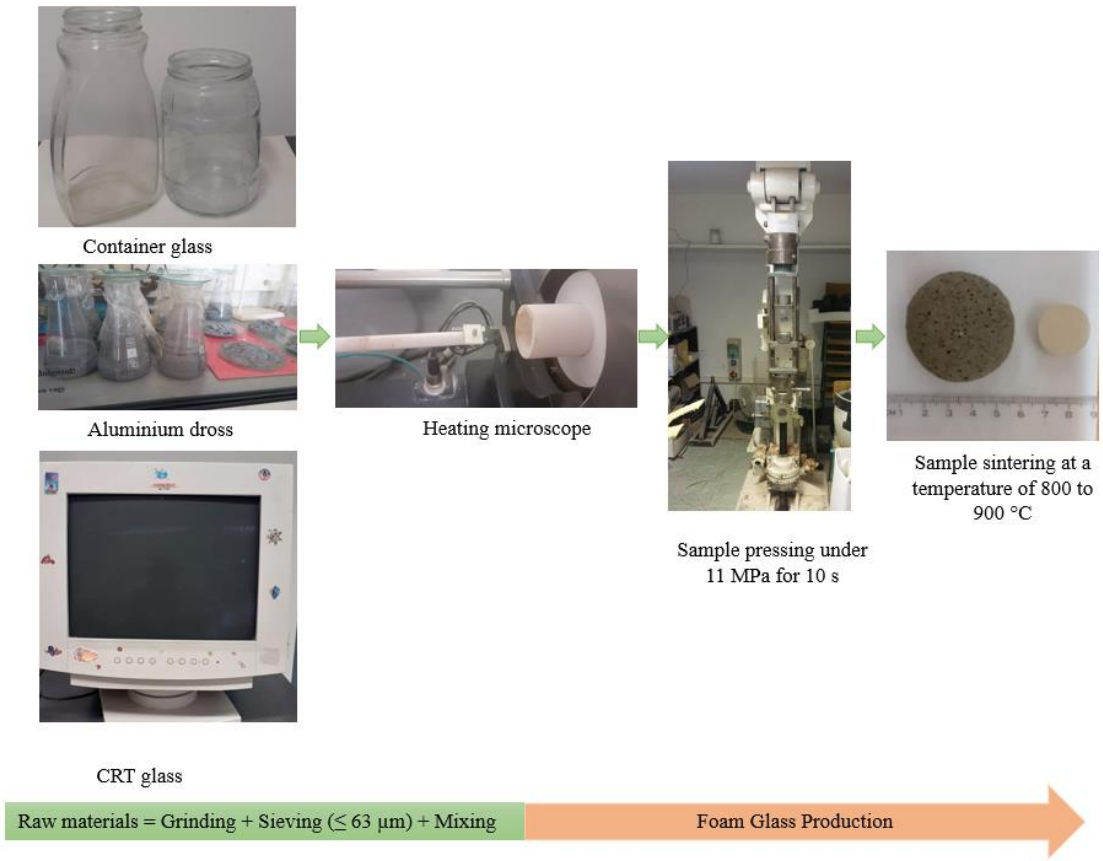

Figure 1. Samples preparation

2.2.Investigation methods

Figure 2 summarizes the methodology followed to investigate foam glass properties. The chemical composition of the container and CRT glasses was determined by X-Ray Fluorescence (Rikagu Supermini). The particles morphology was determined by a scanning electron microscope (SEM) Zeiss EVO MA10. The mineral composition of the dross was investigated by X-ray powder diffractometry (XRD) (Rigaku Miniflex II) and quantified by Rietveld-fitting. After sintering in an electric chamber furnace, the samples were polished into cylindrical shapes (diameter = 40 mm, height = 16.5 mm) where volume expansion, water absorption, bulk density, porosity, microstructure, thermal conductivity, and compressive strength were determined.

Thermal conductivity was determined by a C-Therm TCi using the Modified Transient Plane (conforms to ASTM D7984) [93]. Water absorption was measured under Hungarian standard MSZ EN 1217 B. The compressive strength was measured using an Instron universal testing instrument. The samples were loaded with a force perpendicular to their surfaces.

For the microstructure evaluation, the samples were photographed with Nikon camera and sent to scanning electron microscopy (SEM) with Zeiss EVO MA10 and to computerized tomography scan (YXLON CT computed tomography). The porosity (open and closed pores) was determined through the measurement of the skeletal density and the powder density (ground in mortar) using a Helium pycnometer (ULTRAPYC 1200e, TU Bergakademie Freiberg). To identify foam glass oxides, samples were treated with hydrofluoric acid/perchloric acid and analyzed with Inductively Coupled Plasma Optical Emission spectroscopy (ICP-OES), Spectroflame. Foam glass phases were analyzed using X-ray Powder Diffraction (Siemens Kristalloflex D500), and the results were interpreted by Rietveld-Method. To determine the leaching properties of the material, the leaching test EN 12457-4:2002 was

conducted. To estimate the durability of the foam glass, a hydrolytic resistance of glass grains at 121 °C – (ISO 720:2020 Test methods and classification) was applied.

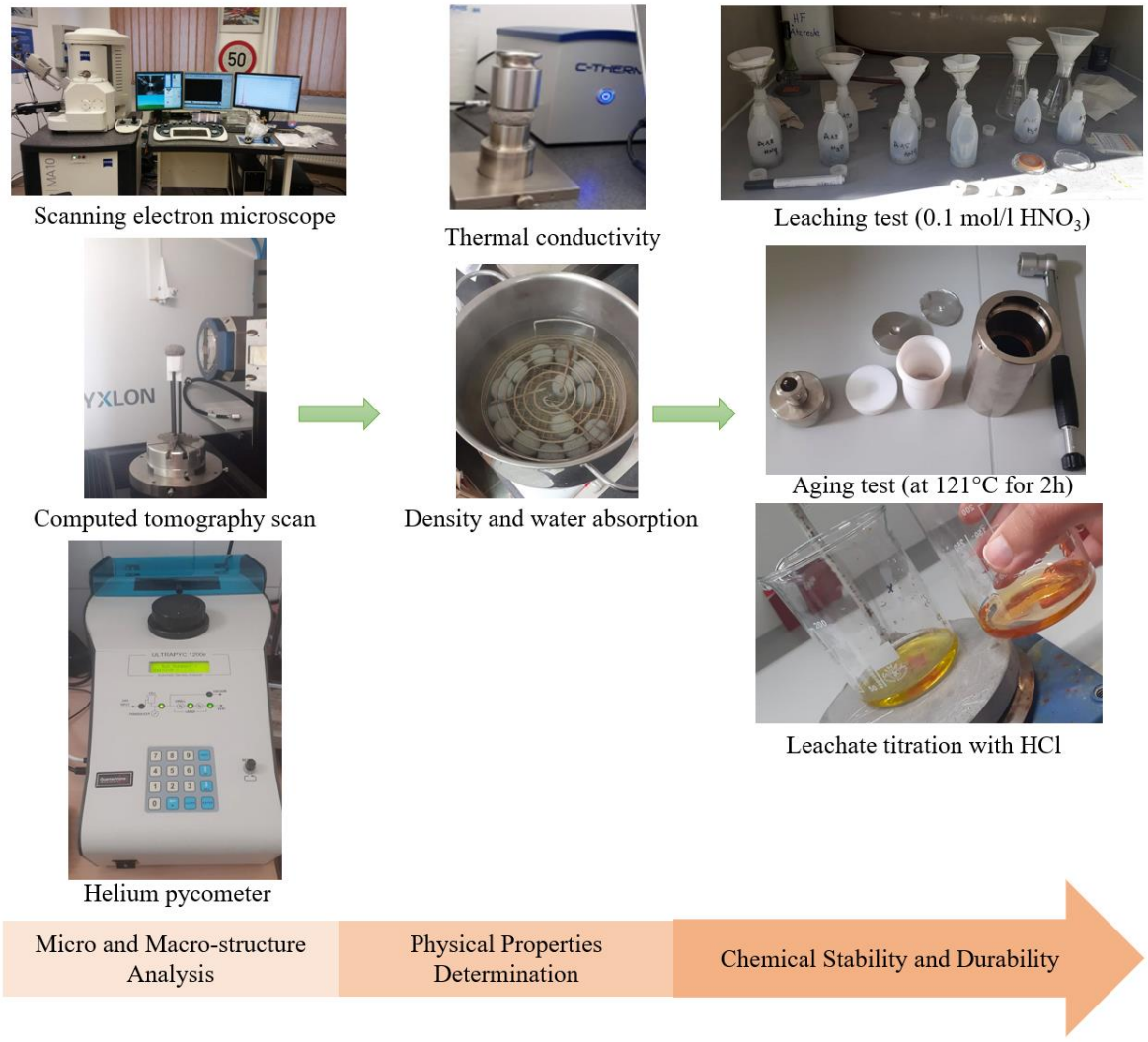

Figure 2. Investigation method

3. Results and discussion

3.1.Sintering and foaming behavior

The foaming behaviour of the mixtures was determined using the heating microscope where the foaming temperature was selected as the temperature associated with the maximum height of the foam (Figure 3). Dross-containing mixtures have a lower foaming temperature and a higher foaming height, while dross-free mixtures show a higher foaming temperature and a lower foaming height. Adding dross decreased the foaming temperature and enhanced the foaming process as it contains AlN responsible for releasing gaseous products (NH_3, N_2, and NO) between 800-920°C [90]. The foaming temperature is decreased by adding alumnium dross due to the salt content (fluorite, halite, and sylvine). There was no pronounced difference between the foaming behaviour of the samples with CRT glass particle size 63 µm and 32 µm.

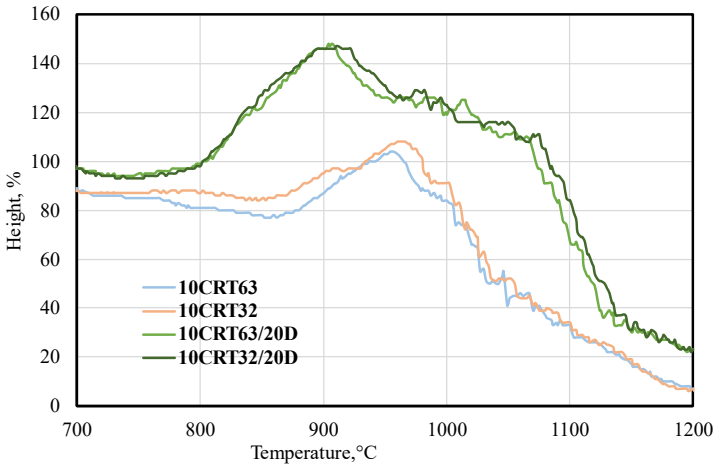

Figure 3. Effect of adding aluminium dross and CRT glass with two particle sizes 63 µm and 32 µm on the foaming process

3.2.Micro and macrostructure analysis

In container glass foams, the cells are small and with a homogenous honeycomb structure. This cellular structure is the result of a highly viscous environment. Adding 5 wt% CRT glass causes a slight increase in the cell size. As the CRT glass content increases to 10 wt%, the cells increase in size and become oval. This is due to the presence of high content of Na_2O, CaO, and BaO provoking non-bridging oxygens and decreasing the viscosity allowing for bubbles to expand during foaming. By adding aluminium dross, the cell size usually increases with increasing the amount of the dross and the heterogeneity increases too. It is due to the boosted foaming effect created by the AlN content besides the low viscosity created by the Na_2O and CaO content leading to cell growth and coalescence (sample G10CRT20D64). If the Al_2O_3 content in the sample composition is higher than the total alkaline content (Na_2O, BaO and CaO) the viscosity will be higher, and the cell size homogeneity is established again (samples G20D64 and G5CRT20D64) (Figure 4 and Figure 5).

CRT / Dross	0 wt%	5 wt%	10 wt%
0D			
	G	5CRT	10CRT
20D64			
	G20D64	G5CRT20D64	G10CRT20D64

Figure 4. Macrographs of the foam glasses (scale=5mm)

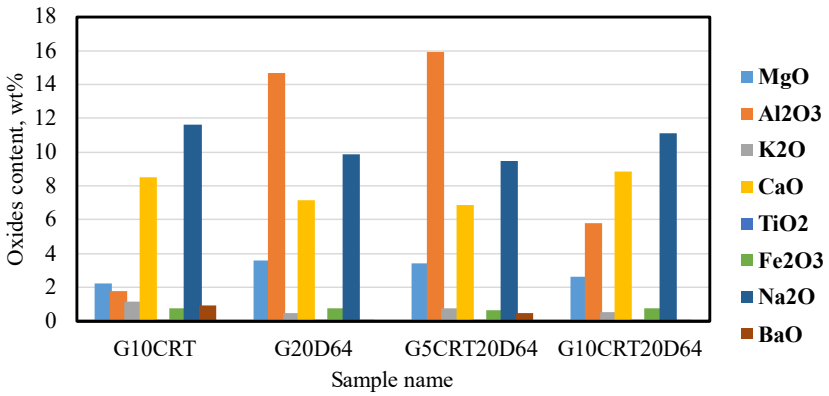

Figure 5. Chemical composition of the foam glasses

3.3.Physical properties

Density and volume expansion

The density of the foam glasses in this study varies from 0.15 to 0.21 g/cm^3 while the commercial foam glasses have a density ranging between 0.13 - 0.3 g/cm^3 [5]. The resultant foam glass can be classified as a lightweight material. The density of the foam glass depends on the foam structure (the size and shape of the cells) and the expansion of the samples. As the volume expansion increses the density decreases (Figure 6). Samples with container glass and dross have slightly lower or equal density to that of the container glass and the lowest densities compared to the other mixtures. The maximum volume expansion is observed in samples with dross types 64 and X (7.8) due to the presence of AlN (10.65 wt% and 19.64 wt% respectively) which enhanced the foaming process. In the other hand, samples with dross 53 have the minimum expansion (7 to 6) due to the low content of AlN in the dross (1.5 wt%).

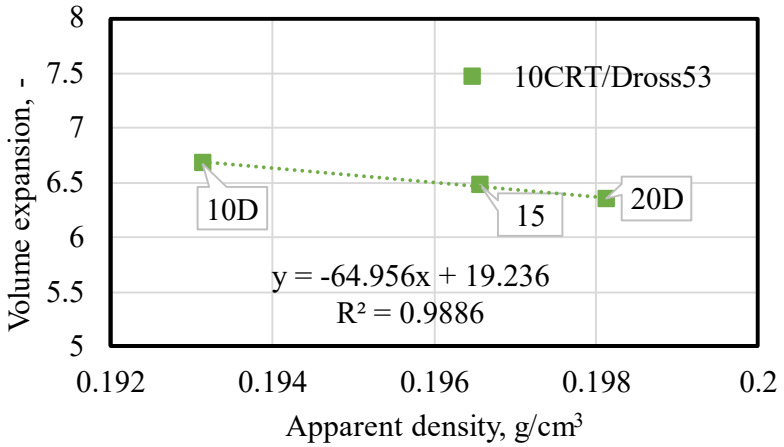

Figure 6. Volume expansion versus apparent density of container glass with 10 wt% CRT glass and dross 53 samples

Porosity and water absorption

In this study, open and closed porosities were found. Dross free samples, exhibit closed porosity and consequently the lowest absorption (15 to 30%) . As the dross content increases, the generation of closed pores decreases causing higher absorption of water. This can be explained by the limited amount of the gaseous substances generated during foaming compared to samples with dross. When the amount of open pores increses the absorption increses too (Figure 7). Samples with dross shows a high absorption tendancy except for samples with 10

wt% CRT. Adding 10 wt% CRT participate in stabilizing the pore structure and limiting the foaming process.

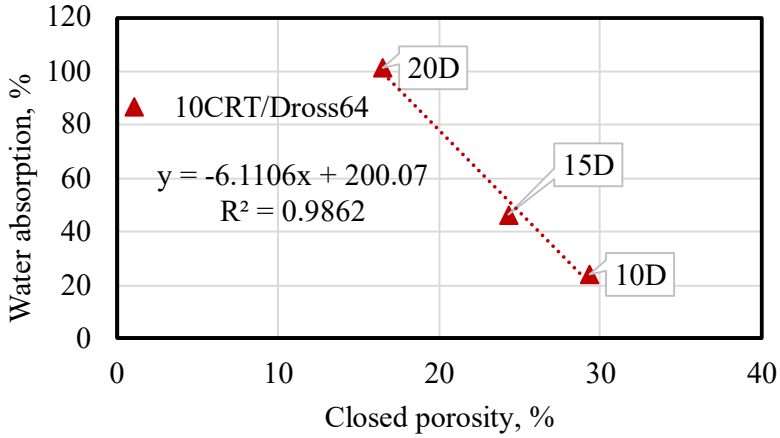

Figure 7. Water absorption versus closed porosity of the foam glass

Thermal conductivity

Thermal conductivity of commercial foam glass ranges from 0.035 to 0.08 W/m·K [5] [6] [7]. The thermal conductivity of the samples ranges from 0.038 W/m·K to 0.055W/m·K which makes them a good thermal insulating material. Homogeneity and cell size affects the thermal conductivity, the more the heterogenous structure and the bigger the cells the lower the thermal conductivity.

Compressive strength

The compressive strength depends on the structure of the foam that will distribute the load. As the porosity increases, the compressive strength decreases (Figure 8). Porosity weakens the load bearing of the foam regardless of the type of porosity (open or closed pores). Another factor that can weaken the foam is the crystal content, due to the dislocation propagation through the plans of the crystal. By introducing amorphous phases to crystalline materials, grain boundaries and phase boundaries can be impeded from moving.

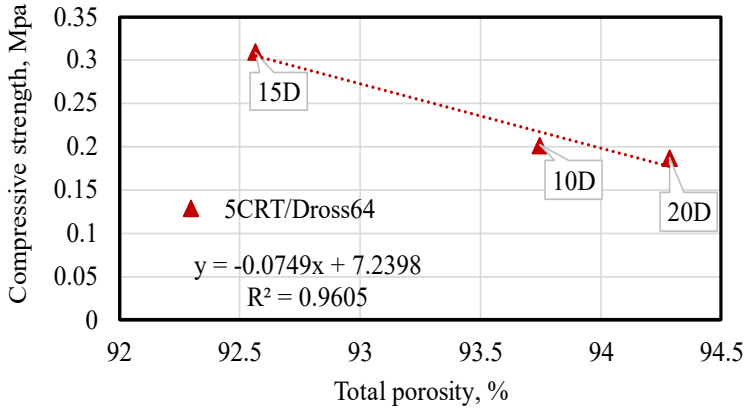

Figure 8. Compressive strength versus the total porosity of the foam glass made with container and CRT glasses and dross 64

3.4.Chemical stability

To determine whether hazardous waste complies with specific acceptable values, the samples with the highest waste material content were selected to undergo the leaching test.

Regardless of the variation of the sample's composition, the hazardous elements concentrations are less than the safe limit of the non-hazardous materials with up to 99 % immobilization.

A thermal cycle was applied on the foam glass to estimate its durability. The cycle is equivalent to 36 months in real-time and was repeated twice. The weight of the samples didn't change significantly in both cycles. There was no alteration in the inside and in the outer surface of the foam glass. The average thermal conductivity didn't tshow any considerably change. This proves that the material properties can last at least 8 years (Figure 9).

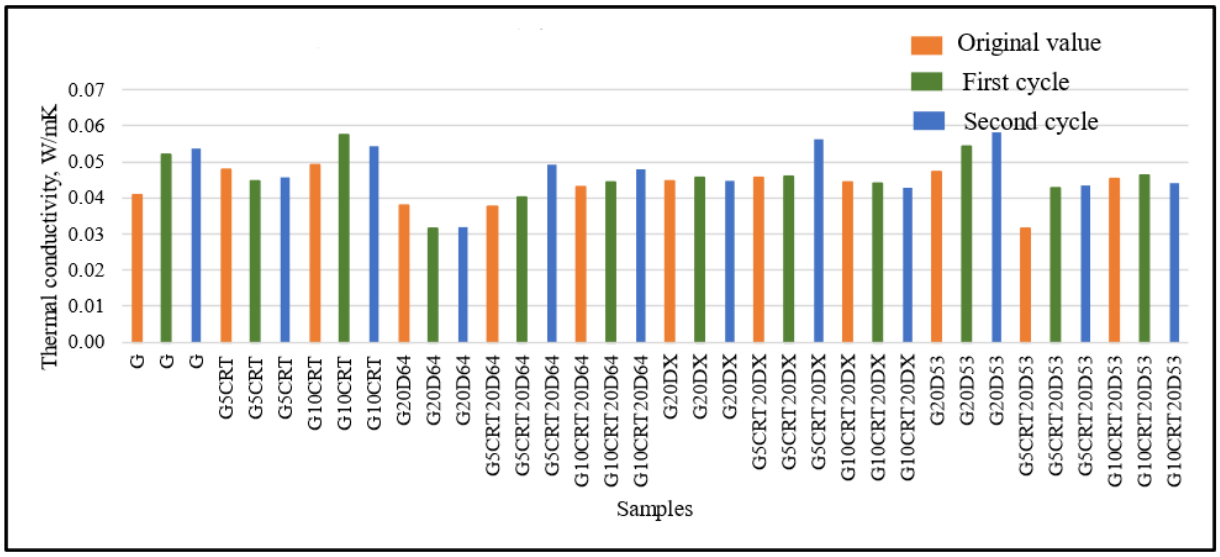

Figure 9. Thermal conductivity deterioration by the aging process

4. Summary

Foam glass was successfully produced using 100% waste materials: container glass material, cathode ray tube (CRT) glass (5 and 10 wt%) with two particle sizes 63 and 32 µm, secondary aluminum dross (10, 15, 20, and 30 wt%), and silicon carbide (2 wt%). The final product is a porous, lightweight material having 0.15 to 0.19 g/cm^3 density, low thermal conductivity (0.038 W/m·K-0.05 W/m·K), suitable compressive strength (up to 0.9 MPa), and appropriate chemical stability (up to 99% immobilisation of the hazardous elements).

5. Claims /New scientific results

Claim on foam glass production based on secondary raw materials

1. Based on the experimental results, I established that foam glass could be successfully produced by using secondary raw materials in the following ranges: 68-98 wt% waste container glass, 5-10 wt% cathode ray tube glass, 10-30 wt% aluminium dross), and 2 wt% silicon carbide as foaming agent. The resultant foam glass is a porous, lightweight material having 0.15 to 0.19 g/cm^3 density, low thermal conductivity (0.038 W/m·K-0.05 W/m·K), suitable compressive strength (up to 0.9 MPa), and appropriate chemical stability (up to 99% immobilisation of the hazardous elements).

Claims on the effect of raw materials on the foaming mechanism

The phase analysis revealed (Table C1) that due to the different composition of the initial aluminium alloys, the treated drosses had similar phases but in different ratios. From the aspect of foaming mechanism, the most important constituents were the AlN and the salt phases.

Table C1. Mineral composition (wt%) of the aluminium drosses (XRD analysis)

Phase name and formula	**Dross type**		
	64	**X**	**53**
Spinel ($MgAl_2O_4$)	22.54	23.49	54.76
Wurtzite (AlN)	10.65	19.64	1.5
Corundom (Al_2O_3)	6.77	14.18	12.6

Phase name and formula	Dross type		
	64	X	53
Nordstrandite ($Al(OH)_3$)	18.01	11.82	17.03
Bayerite (β-$Al(OH)_3$	39.25	-	8.98
Calcite ($Ca(CO_3)$)	-	-	2.62
Calcite Magnesium $(CaMg)(CO_3)$	-	7.39	-
Halite (NaCl)	8.71	13.58	1.79
Fluorite (CaF_2)		9.9	0.56
Sylvite (KCl)	-	-	0.17
Salts together	8.71	23.48	2.52

Heating microscopy was used to characterize the foaming behaviour of the materials. In this method the foaming temperature was defined as the temperature where the sample reached the maximum height.

2.1. I established that aluminium drosses having more than 10 wt% aluminium nitride (AlN) content (lines dross X, dross 64 on Figure C1) possess a self-foaming mechanism due to the decomposition of AlN in which gaseous products are released. The decomposition takes place at a temperature between 800-920°C and drives the expansion of the foam. In the lack of AlN (line dross 53 on Figure C1), the foaming process is less intensive as only the decomposition of SiC assists it.

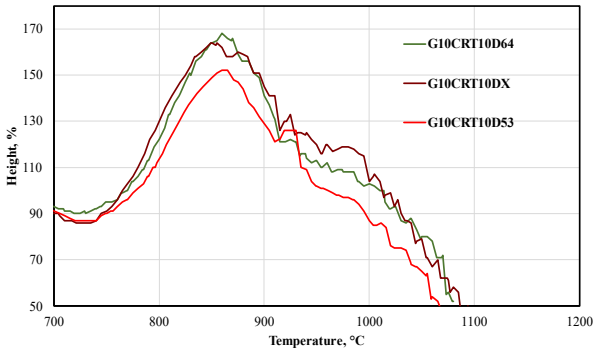

Figure C1. Effect of the aluminium dross types (X, 64, 53) on the foaming behaviour

2.2. I established that there is no significant difference between mixtures with 63 µm particle size of the CRT glass and those with 32 µm particle size (Figure C2-line CRT63 and -line CRT32). Combining the two-particle sizes of the CRT may decrease the foaming height from 145% to 120%. By using two different particle sizes, the voids between particles may be filled, thereby reducing the amount of oxygen in the sample and limiting the oxidation reaction during foaming (Figure C2-line CRT32-63).

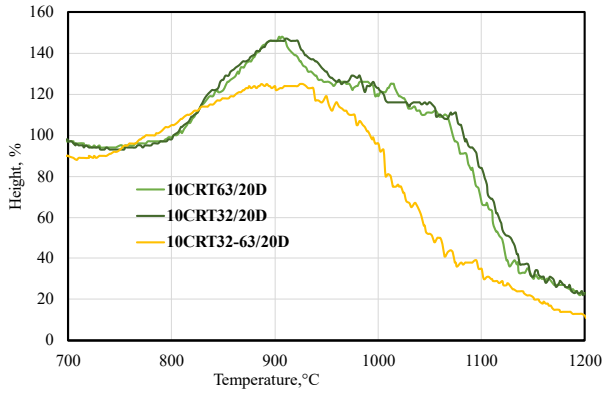

Figure C2. Effect of CRT glass particle size on the foaming process

2.3. I established that the salt content (NaCl, KCl, CaF_2) also affects the foaming behaviour as salts lower the foaming temperature due to the fluxing effect of alkalis. In sample G10CRT20DX with the highest salt content (23 wt%), there is a 20°C reduction in the foaming temperature compared with the sample (G10CRT20D53) having 2.52 wt% salt content (Table C2).

Table C2. Effect of salt content on the foaming temperature

Sample name	Salt content (wt%)	Foaming temperature (°C)
G10CRT20D64	8.71	859
G10CRT20DX	23.48	845
G10CRT20D53	2.52	865

2.4. CRT glass has almost the same composition as container glass except the hazardous element. Lead is the most abundant hazardous element beside barium (2342 ppm). I established that the lead content of CRT glass lowers the melting temperature of the glass due to the existence of lead presented in CRT glass as bivalent Pb^{2+}. The polarizability of this cation can further decrease the viscosity across a wide range of temperatures by creating non bridging oxygens. It can be seen in Figure C3 where CRT-free sample (G15D64) has higher foaming temperature (869 °C) than the sample G10CRT15D64 having 10 wt% CRT glass (855°C).

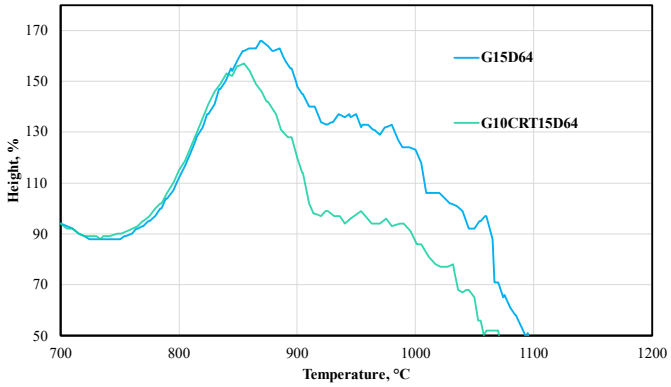

Figure C3. Effect of lead in CRT glass on the foaming behaviour

Claims on the effect of the raw materials on the viscosity of glass mixtures and volume expansion

The viscosity is one of the most important properties of the glass, as it determines the behaviour of the glass during the melting. It can be directly measured or calculated from the oxide composition of the glass. The components of a glass are classified as network formulating, modifying or intermediate. The stability thus the viscosity of the glass network is based on the ratio of bridging and non-bridging oxygens. Besides the foaming agent, the viscosity of the glass affects the expansion process of the foam. One way to characterize the viscosity is through determining the final composition of the foam glass (Figure C4).

3.1. I established that dross-free samples contain sodium oxide as a major component followed by calcium oxide, magnesium oxide, aluminium oxide. Usually, high concentration of Na_2O and CaO (Na_2O+CaO= 20 wt%) creates more non-bridging oxygens resulting in decreasing the viscosity and allowing gas bubble formation. Further decrease in the viscosity may provoke gas escaping and destruction of the bubbles. The high amount of Al_2O_3 in aluminium dross 64 (16 wt%-Figure C4) causes a decrease in the number of non-bridging oxygens, resulting in higher viscosities. If the amount aluminium, calcium, and sodium oxides are similar, it can create an equilibrium effect on the viscosity to create a more stable foam structure.

3.2. Due to its PbO content, adding CRT glass has an extremely strong viscosity-lowering effect by acting as a modifier. Lead weaknesses the network by creating non-bridging oxygen while due to its size, its migration is limited.

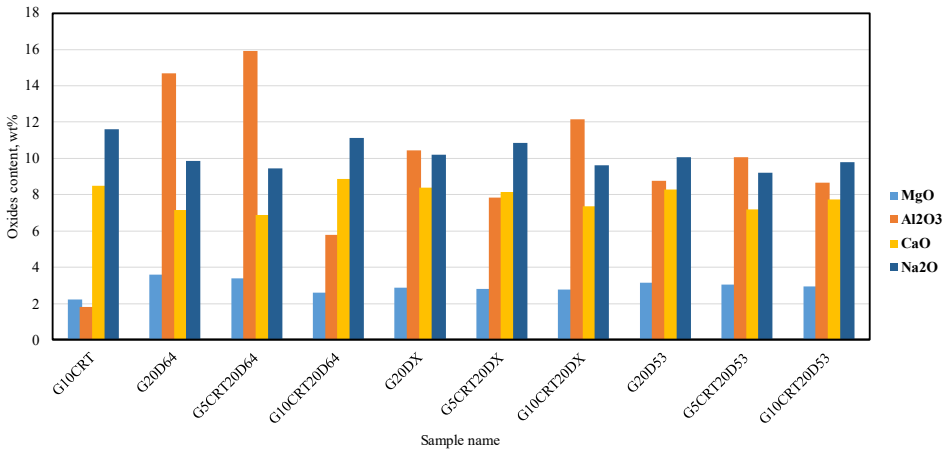

Figure C4. MgO, A_2O_3, CaO, and Na_2O content in foam glasses

3.3. I established that the maximum volume expansion is detected in samples with dross types 64 and X (volume expansion coefficient=7.8) due to their high AlN content (10.65 wt% and 19.64 wt%, respectively) which will boost the foaming process.

3.4. Due to the low AlN content (1.5 wt%) in dross 53, samples with dross 53 have the minimum expansion (7 to 6), which hinders the foaming. Besides, when CRT glass content is increased, foam growth is restricted during sintering, resulting in a more homogeneous pore distribution. It is related to the high viscosity generated due to the high alkali content especially with 10 wt% CRT glass leading to bubble collapse during foaming.

3.5. If the glass foams are insufficiently heated or the viscosity is high, gas bubbles will not be generated. On the contrary, the outer shell of the pores collapses if the viscosity is low or the foaming process is too intense, resulting in bubble fusion. The key to prevent bubbles from limited growth or overgrowth is controlling the aluminium nitride content and alkali oxides to create a suitable viscosity for bubbles generation.

Claims on cell size characterization

Foam glass's cell structure will determine its physical properties, mainly density, thermal conductivity, and compressive strength. Herein, cell size, geometry, orientation, distribution, and type of connectivity are the key features for the characterization of foam glass. A full description of the cellular system is essential to explain not only the properties of the foams but also the viscosity environment at the exact foaming temperature. From the CT data of the cell sizes detected, I calculated the average, maximum, and minimum cell sizes. I used statistical data analysis of the cell size and distribution generated by the CT scan and linked it to the oxide's component of the foam glass to understand the effect of Al_2O_3, CaO, Na_2O, BaO, and Pb on the glass structure.

4.1. I determined that the mode indicated the most frequent cell size, and the standard deviation (SD) reflected the degree of dispersion of the cell sizes. An SD value close to 0 or to 1 indicates a homogenous or a heterogeneous cell structure, respectively. This can be seen in Figure C5 where foam glass with container glass has a homogenous structure with a standard deviation of 0.28 while sample G10CRT10D64 has a heterogenous cell distribution which can be seen in the macrograph and in the standard deviation value (0.714).

Sample G with SD=0.28

Sample G10CRT10D64 with SD=0.714

Figure C5. Macrograph of the sample made with container glass and the sample made with 10 wt% CRT and 10 wt% dross 64

4.2. I established that samples with only container glass and samples with 5 wt% CRT glass had almost the same homogenous cell structure with a maximum and a minimum cell size around 3.1 mm and 0.1 mm, respectively (Table C3). It is due to the high viscosity environment which gives limited access for bubbles to growth. Increasing the CRT glass to 10 wt%, the maximum cell size increased to 5.496 mm and the standard deviation (SD) increased to 0.714 so the cell distribution tends to be heterogeneous. This increase may be due to the presence of high content of Na_2O, CaO, and BaO responsible for creating non-bridging oxygens and consequently decreasing the viscosity. Lower viscosity will allow the creation of bigger bubbles and heterogeneous structure (Figure C6).

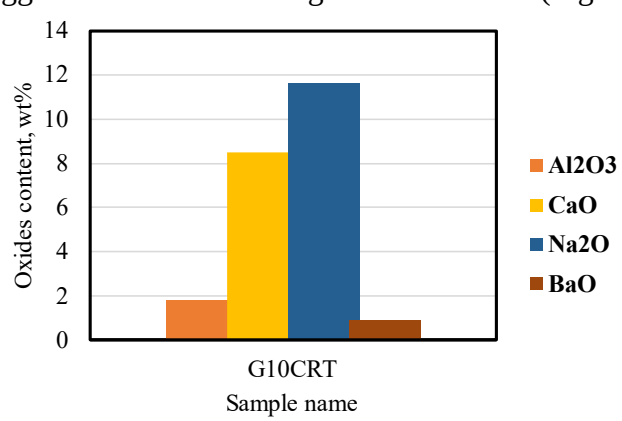

Figure C6. Main oxide composition and macrograph of the sample G10CRT

Table C3. Statistical parameters of the cell size distribution determined from the 2D CT scan

	G	G5CRT	G10CRT
Average (mm)	0.719	0.793	0.758
Median (mm)	0.716	0.565	0.475
Mode (mm)	0.736	0.303	0.273
Maximum (mm)	3.126	3.180	5.496
Minimum (mm)	0.161	0.141	0.131
Standard deviation, SD	0.285	0.528	0.714

Claims on the effect of dross composition on the cell sizes

Aluminium dross composition varies depending on the initial source. Besides aluminium nitrides, the main dross oxides that can affect the properties of foam glass are Al_2O_3, CaO, Na_2O, and MgO. Since MgO content didn't seem to change in the samples (an average of 3.5 wt%), it is considered a component of the network formation and excluded in this study.

5.1. I established that adding aluminium dross to container glass increased the maximum cell size from 3.1 mm to 7 mm in samples with 10 wt% dross. The higher the dross content in the sample, the wider spherical pores appear in the center due to the boosted effect of the foaming process generated by the high AlN content (10.6 wt%) leading to cell growth and coalescence. The most frequent cell size in container glass sample reported to be 0.7 mm while the most frequent cell size in samples with dross or dross and CRT is around 0.2 mm to confirm that adding aluminium dross increases both cell size and the number of small pores within the walls, resulting in an enhanced heterogeneity in the structure of the foam glass (indicated by SD=0.747) (Table C4). Samples with high amount of Al_2O_3 (16 wt%) (Figure C7) have rounder and smaller cells indicating high viscosity environment compared to the sample containing higher alkaline oxides ($CaO+Na_2O$=20 wt%) with bigger agglomeration of cells (Figure C8). Both samples contain the same amount of dross but different amount of CRT glass. In this case, increasing CRT glass content created a less viscous environment which cause the bubble to collide and agglomerates to create bigger cells.

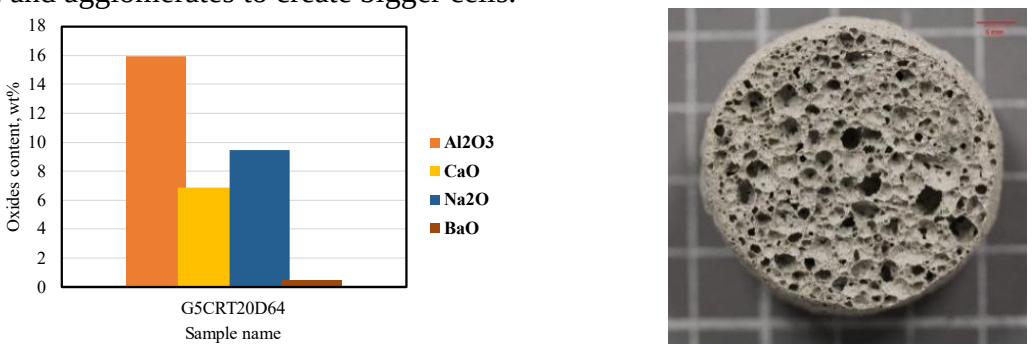

Figure C7. Main oxide composition and macrograph of the sample G5CRT20D64

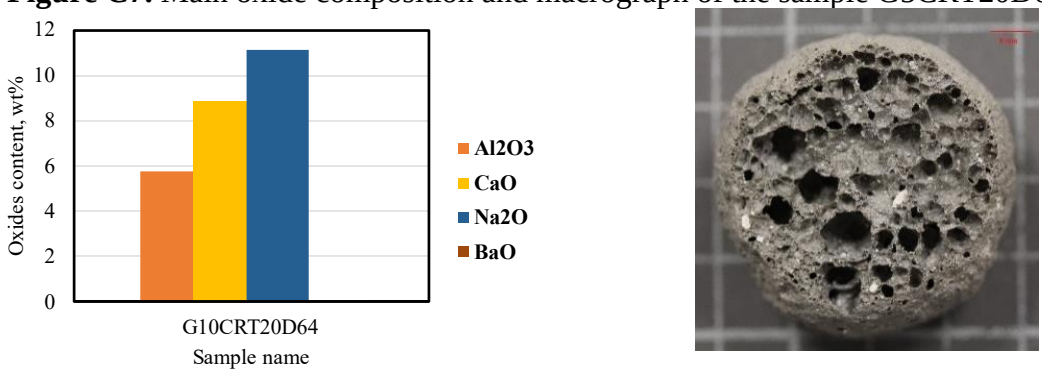

Figure C8. Main oxide composition and macrograph of the sample G10CRT20D64

5.2. I established that samples with container glass and 20 wt% dross X exhibit large heterogeneous cell sizes suggesting a low-viscosity environment (Figure C9). Since the amount of Na_2O equals Al_2O_3, the effect of those ions on the viscosity will be nullified. However, the effect of the alkali ions will be boosted since the presence of CaO will decrease the viscosity of the melt. Sample G10CRT20DX has wider cells (Figure C10). It is explained by the high content of Na_2O, BaO, and CaO (18 wt%) compared to Al_2O_3 content (12 wt%), which results in the destruction of the bridging oxygens in the glass structure and lowering the viscosity.

Table C4. Statistical parameters of the cell size distribution determined from the 2D CT scan

	G10D64	G5CRT10D64	G10CRT10D64
Average (mm)	0.622	0.692	0.681
Median (mm)	0.384	0.433	0.443
Mode (mm)	0.264	0.312	0.272
Maximum (mm)	7.227	6.059	7.543
Minimum (mm)	0.024	0.131	0.030
Standard deviation	0.649	0.657	0.747

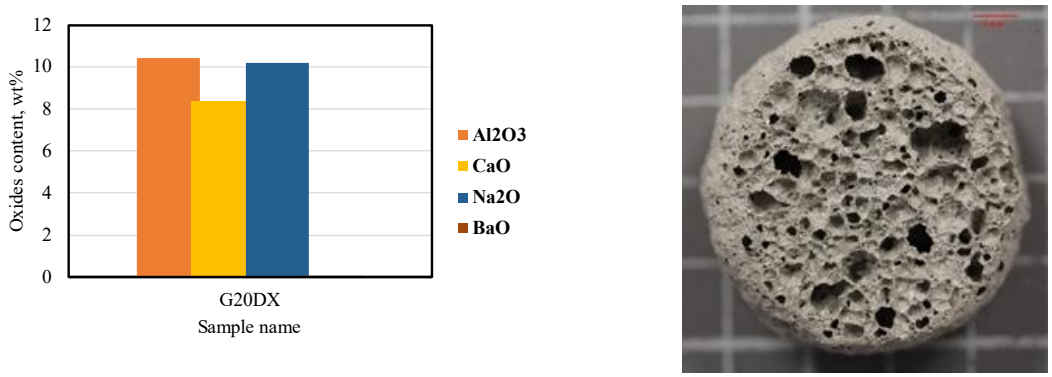

Figure C9. Main oxide composition and macrograph of the sample G20DX

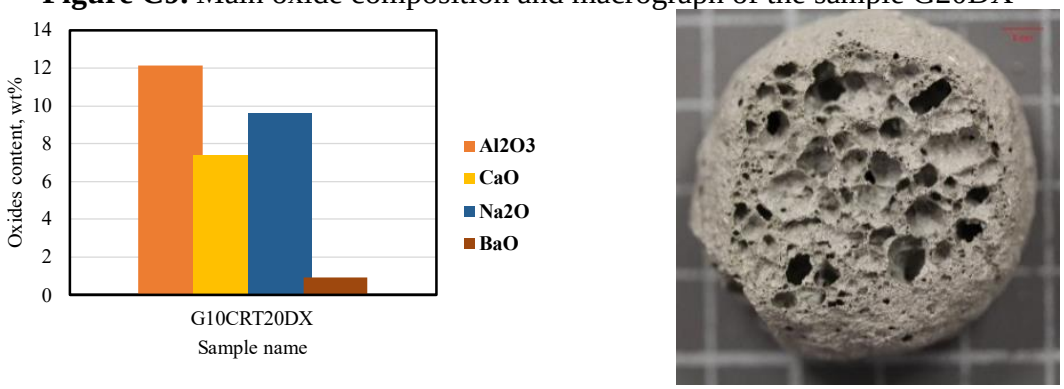

Figure C10. Main oxide composition and macrograph of the sample G10CRT20DX

5.3. I established that adding aluminium dross 53 will create a homogeneous cell structure compared to the previous two types of dross. It may be explained by the limited effect of the AlN rather than by the effect of the alkali ions (Figure C11). In the counterpart, samples with 20 wt% dross and 10 wt% CRT glass, shows an increase in the cell size, and the structure becomes more heterogeneous (G10CRT20D53) (Figure C12). It is due to high content of Na_2O and CaO content (19 wt%) which decreases the viscosity, the viscous forces created are exerted on the bubble, causing it to break. Even with the low AlN content (1.5 wt%), a high amount of dross X combined with 10 wt% CRT glass content may boost the foaming process due to the alkali content which decreased the viscosity allowing for bubble formation to create big cells.

Figure C11. Macrograph of the sample G5CRT10D53

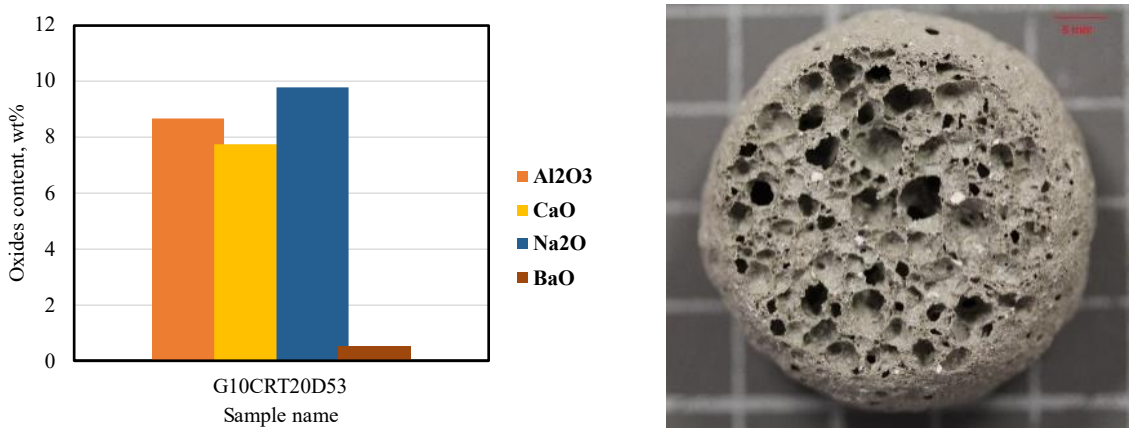

Figure C12. Main oxide composition and macrograph of the sample G10CRT20D53

Claims on the type and shape of the pores

I established that adding CRT and dross will not only change the cell size but also cell shapes, connectivity and the intercell in the walls.

6.1. Foam glass made with container glass has mostly sub-millipores (0.1 and 1 mm) that are more tetrahedra hexagons than round. The walls of the cells contain oval super-micropores (10 to 100 μm). Those oval super-micropores have walls containing sub-micropores (0.1 to 1 μm). This can indicate a high viscosity growth environment.

6.2. Sample with 5 wt% CRT has oval sub-millipores that appear surrounded by a high number of round super-micropores. The millipores were deeper than in the container glass foam which may indicate open porosity. Adding 10 wt% of CRT glass results in slightly larger inter-millipores (1 to 10 mm) where their walls contain a smaller amount of super-nanopores (10 to 100 nm) compared to the other samples.

6.3. A sample containing container glass and dross 64 shows mostly inter-millipores, as well as -inter-micropores linked together. The walls of the inter-micropores are formed by alignment of nanopores. The concave part of the pore displays a needle structure that may indicate the existence of a crystallized phase. The CT scan results proves that adding aluminium dross will generate higher nanopores which can be seen in the micrographs (Figure C13).

6.4. AlN in dross boost the foaming process to generate more irregular pores while other compounds will act as counteracting effects to increase the viscosity, such as aluminium oxides, which will slow down the foaming process and generate rounder smaller cells.

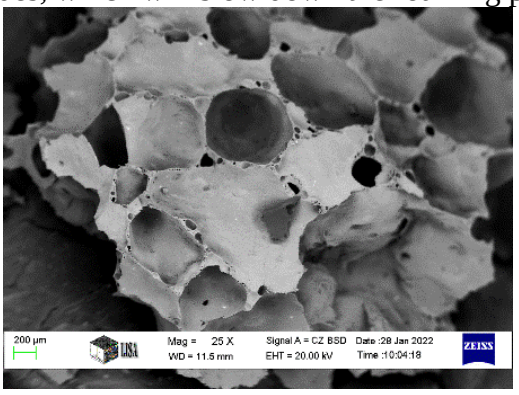

G

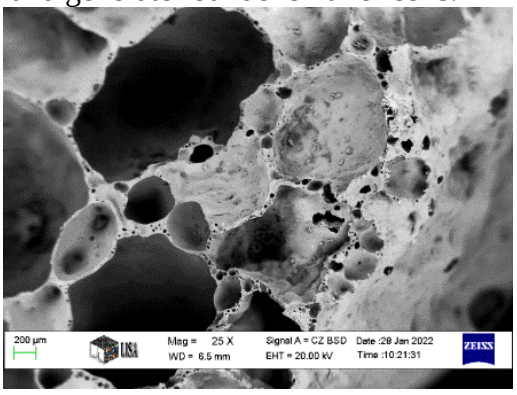

5CRT

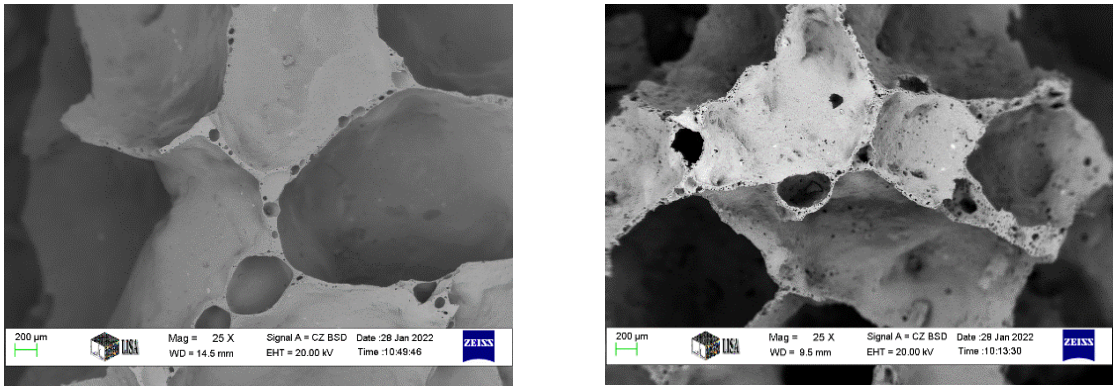

10CRT G10D64

Figure C13. Micrographs of the foam glasses

Relationship between the Al_2O_3/Na_2O ratio, the density and the amount of raw materials

I established that the density of foam glass depends on the cell structure (the size and shape of the cells) and the amount of dross and CRT glass added. Secondly, I excluded the mixtures with 30 wt% dross content due to the high density generated (0.9 g/cm^3) and focused on using 10 to 20 wt% dross and study the effect of using drosses with different composition.

7.1. Firstly, I revealed that the average cell size is highly (R^2= 0.9095) negatively correlated to the density of the foam glass (Figure C14).

$$y = -0.4741x + 1.286$$

As the aluminium dross content increases the average cell size of the foam decreases and the density increases. It is due to the indirect effect of the dross oxides on the viscosity and thus the foaming process.

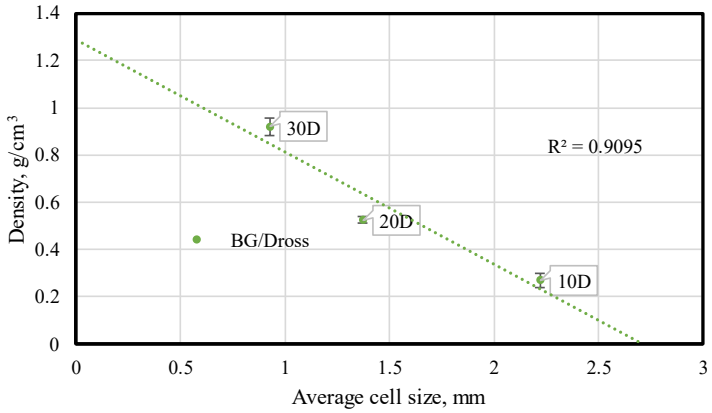

Figure C14. Density versus average cell size of foam glass made with container glass and dross

7.2. I established that the ratio of Al_2O_3/Na_2O used to determine the density behaviour in soda lime silicate glass can be applied to foam glass with dross X and 53 where the density will decrease as the Al_2O_3/Na_2O ratio increases to 1.2, then starts to increase again.

7.3. Despite the low amount of Al_2O_3 in the sample G10CRT20D64 (5.5 wt%) allowing the alkali oxides to act and create lower viscosity and bigger cell sizes, the density is high. It may be related to the presence of a high amount of CaO (8 wt%) which tends to increase the density.

7.4. Not only the Al_2O_3 and Na_2O content will affect the density but also the volume expansion, porosity and the cell size. As it can be seen in Figure C15, the apparent density is highly (R^2=0.9886) negatively correlated with the volume expansion as follows:

$$y = -64.956x + 19.236$$

The density of samples increases as the amount of dross content increases which will decrease the expansion process of the sample.

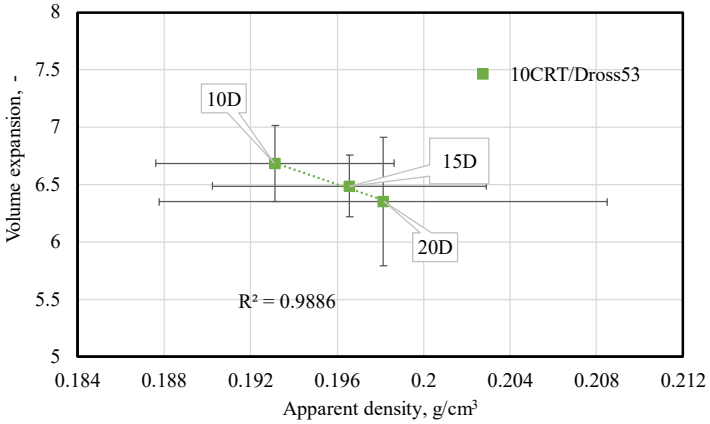

Figure C15. Volume expansion versus apparent density of samples with container glass, 10 wt% CRT, and Dross 53 (10CRT/Dross 53)

Effect of pore types and cell structure on the water absorption

There are two types of foam glass: water-resistant and still absorbing mist and humidity, and high-absorption material used for drainage. It depends on the type of pores formed. Pores that are open to the outside are known as open pores. It is generated in high viscosity environment where the separating walls are not completely formed. On the other hand, closed pores can be the product of two phenomena. The first is caused by intensive heating, which results in the collapse of parts near the pores' outer shell. The second reason is due to the insufficient evolution of gaseous substances. I established that both high and low absorption foams can be generated depending on the initial composition.

8.1. Dross-free samples have the lowest absorption values (13 to 35 %), whereas container glass with 5 wt% CRT glass has the lowest absorption (13 %). It may be caused by the intensive heating, resulting in the outer shell collapsing, or due to the insufficient evolution of gaseous substances during foaming, which seems to be the cause as dross-free samples doesn't contain AlN, so the foaming process is limited.

8.2. Samples containing 10 wt% CRT and 10 wt% dross have the lowest water absorption (20 to 24 %) compared to the other samples with dross. Adding 10 wt% CRT contributes to stabilizing the pore structure and limiting the foaming process.

8.3. Water absorption can be linearly correlated (R^2=0.9862) with the closed porosity and dross content as follows:

$$y = -6.1106x + 200.07$$

As the dross content increases, the generation of closed pores decreases causing higher absorption of water (Figure C16).

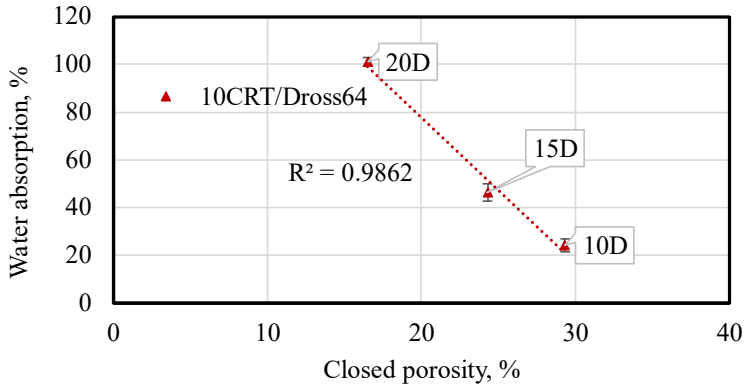

Figure C16. Water absorption versus closed porosity of the foam glass in 10CRT/Dross64 samples

Claim on cell size, homogeneity, and thermal conductivity relationship

The thermal conductivity of a material is the amount of heat transferred through its surface due to a temperature difference. Material with a lower thermal conductivity resists heat transfer better, so it is more effective as an insulation. If gases can be trapped, they make good insulation materials since they have poor thermal conduction properties which is the case of foam glass.

9.1. I established that the average cell size and wall thickness can directly affect the thermal conductivity of the foam glass. As the average cell size increases the thermal conductivity decreases (R^2=0.946):

$$y = -0.0135x + 0.0699$$

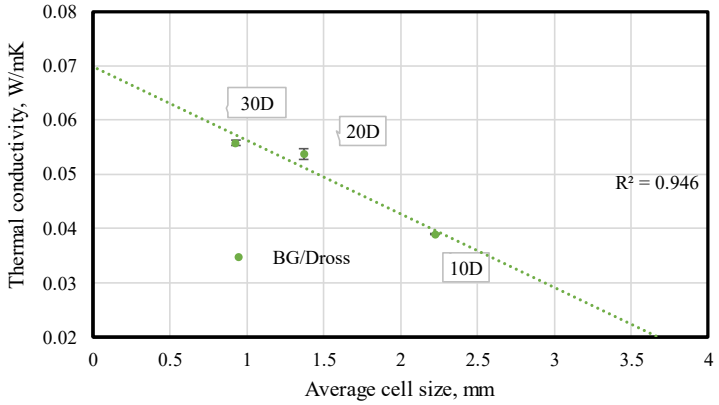

Figure C17. Thermal conductivity versus the average cell size

9.2. I established that the homogeneity of cell's structure affects directly the thermal conductivity. As the standard deviation indicates the homogeneity of the foam glass structure, a heterogeneous cell size distribution will give better thermal insulation. G10CRTD64 foam glass has a heterogeneous cell structure (SD=0.7) and is the least thermally conductive. Herein, the heat flow propagates usually through solids, so the flow will only propagate through the walls. If the walls are thin and contain high number of pores, the heat flow will be attenuated (Figure C18).

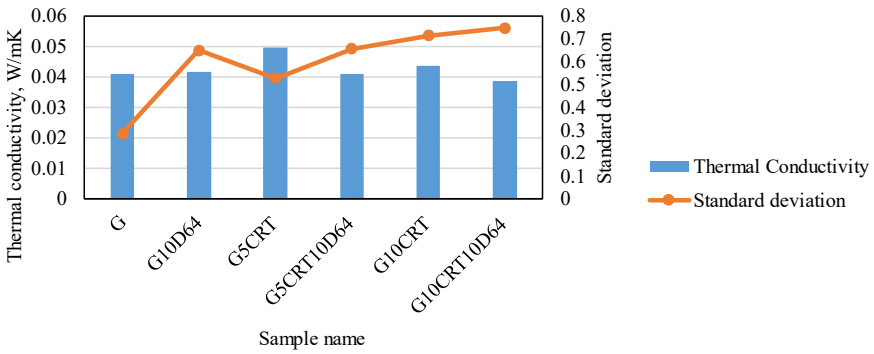

Figure C18. Thermal conductivity versus standard deviation of the cell size

Claims on the effect of foam structure phases on the compressive strength

Foam glass is typically used in road, harbour, bridge, ramp, and culvert foundation work because it reduces loads on the soil as well as horizontal loads on structures. This led to the necessity to investigate the foam glass compressive strength.

10.1. I established that the compressive strength is related to the structure of the foams rather than the crystals content. Samples with dross 64 have the weakest compressive strength which decreases with increasing the amount of dross. As cell size increases the ability to withstand load will further be weak. On the other hand, samples with dross 53 have high compressive strength, due to their well-packed structure that can divide and distribute the applied force between the cell walls. The low compressive strength of samples containing dross 64 compared to the other two types of dross may be explained by the high amount of crystal phases present. Dislocation usually, propagates through the crystal plan. By introducing amorphous phases to crystalline materials, grain boundaries, and phase boundaries can be impeded from moving.

10.2 The hardness of the total phases (Table C5) will determine the hardness of the foam. Samples containing dross 53 and X will have the highest hardness (6-7), followed by dross 64 (6 to 6.5) and dross-free samples G10CRT (5-5.5). Neither can be true since the sample G10CRT has a higher compression strength than the samples with dross 64 and 10 wt% CRT glass. For foam glass, the hardness of the phases doesn't apply.

Table C5. Effect of hardness and number of mineral phases on the compressive strength

Sample	Mohs hardness	Compressive strength (MPa)	Number of phases
G10CRT20D53	6.5-7	0.5	5
G10CRT20DX	6-7	0.5	6
G10CRT20D64	6-6.5	0.2	8
G10CRT	5-5.5	0.5	6

10.3. I revealed that the compressive strength of foam glass was highly correlated (R^2=0.9605) with its porosity independently of its dross content (Figure C19) according to the following equation:

$$y = -0.0749x + 7.2398$$

As porosity increases, the compressive strength decreases. Porosity weakens the load-bearing capacity of the foam regardless of the type of porosity (open or closed pores).

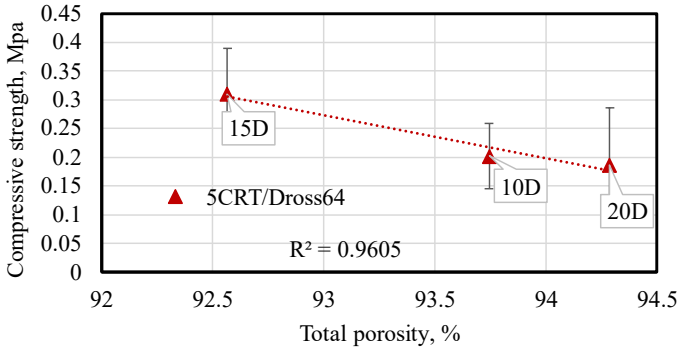

Figure C19. Compressive strength versus the total porosity of the foam glass made with container glass and dross 64 (5CRT/Dross64)

Claims on the leaching characteristics

To determine whether hazardous waste complies with specific acceptable values, the samples with the highest waste material content were selected to undergo the leaching test. The leaching behaviour of the hazardous elements was observed.

11.1. I established that the leaching rate of the hazardous elements is extremely low with immobilisation up to 99 %. For example, the lead concentration in the eluates was below the safe limit (≤10 ppm) for all samples (Table C6), resulting in a Pb immobilization of up to 99% (minimum immobilization = 95%). This indicate that the lead is trapped in a crystal phase rather than the glassy phase.

Because of its small amount, lead can become trapped in iron-containing crystal phases without being detected by the XRD. The crystal phase is probably magnetite [104], as it is observed in the XRD results.

Table C6. Lead content in foam glass and in leachate

Sample code	Lead in foam glass (ppm)	Lead leached (ppm)	Lead immobilisation (%)
G20D64	33	1.16	99.61
G5CRT20D64	139	0.77	98.92
G10CRT	315.7	1.20	96.19
G10CRT20D64	18.17	0.01	99.99
G20DX	16.08	1.66	99.73
G5CRT20DX	181.3	0.96	98.25
G10CRT20DX	307.9	1.53	95.30
G20D53	7.6	0.25	99.99
G5CRT20D53	293	1.38	95.94
G10CRT20D53	190.9	1.69	96.77

Chemical durability and aging observation and prediction

As there was no specific test to determine the durability of the foam glass, I used the standard for the hydrolytic resistance of glass grains (ISO 720:2020) which seems the harshest test. I applied a specific thermal cycle to accelerate the weathering test (1 cycle = 36 months in real-time). Dross-free samples and samples with the highest dross content (20 wt%) and 5 to 10 wt% CRT were selected to undergo this test.

12.1. The weight and thermal conductivity of the samples didn't change. There was no alteration on the inside or outside surface of the foam glass and the average thermal conductivity didn't exceed 0.06 W/mK. This proves that the product can withstand up to 8 years before its properties start to degrade.

12.2. Using the accelerated weathering data, I established to build a forecast of the thermal conductivity estimation of 20 years from now. The prediction was done using the forecast function in Excel by using linear regression where in the worst case, the thermal conductivity may reach 0.07 W/mK which considered still in the range of insulation material (Figure 20).

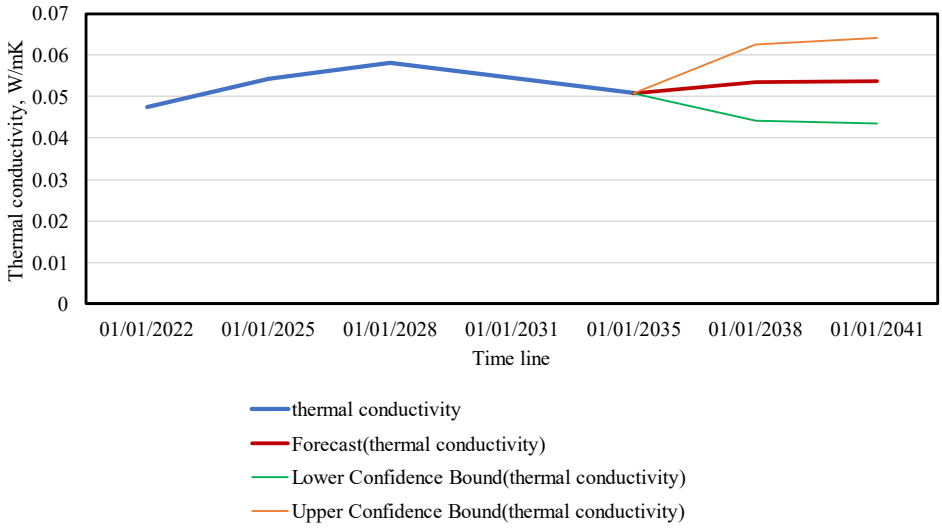

Figure C20. Thermal conductivity deterioration forecast

12.3. I applied a more vigorous cycle to two samples of G20D53 using nitric acid at a high temperature (200 °C). There was no weight loss (5 g), the structure was preserved, and no alteration occurred. The sample with water shows high white efflorescence due to the dissolved salts while samples in nitric acid show both efflorescence and oxidation. The thermal conductivity increased to reach 0.048 W/m·K in the sample immersed in water and further increased to reach 0.05 W/m·K in the sample placed in acid (Figure C21 and C22).
The foam glass has excellent chemical stability against acids which will help with liquid waste disposal.

(A) **(B)**

Figure C21. G20D53 sample in water - efflorescence (total dissolved salt) (A), Sample in acid - efflorescence (total dissolved salt) + oxidation (B)

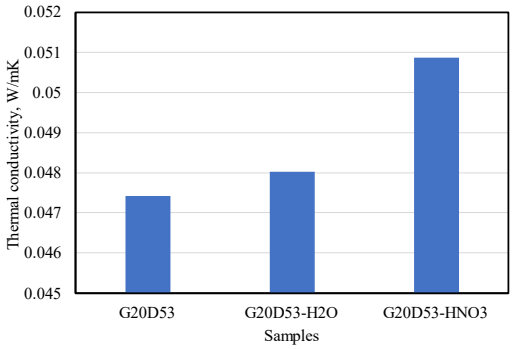

Figure C22. Thermal conductivity deterioration of the foam glass G20D53 under severe conditions

6. List of publications

Journal article

M. Sassi and A. Simon, "Waste-to-Reuse Foam Glasses Produced from Soda-Lime-Silicate Glass, Cathode Ray Tube Glass, and Aluminium Dross," *Inorganics*, vol. 10, no. 1, p. 1, 2021.

Conference Proceeding

1- Y. Illés, M. Sassi, H. Zakiyya and T. Kékesi, "Fluoride Salts from Secondary Aluminium Dross The Fundamental Kinetic Characteristics of Aqueous Dissolution of Chloride and," in International Multidisciplinary Scientific Conference, Miskolc, 2019.

2- M. Sassi, J.-E. F. M. Ibrahim and A. Simon, "Characterization of foam glass produced from waste CRT glass and aluminium dross," in Journal of Physics Conference Series, Miskolc, 2020

Oral Presentations

1. M. Sassi, Foam glass made by container glass, cathode ray tube glass and aluminium dross ISCAME international conference, Debrecen, Hungary, 2019
2. M. Sassi, Foam glass production based on container glass cathode ray tube glass and aluminium dross, Conference EC-Siliconf 1 International Conference, Lillafüred, Hungary, 2019
3. M. Sassi, Characterization of foam glass produced from waste materials, Conference EC-Siliconf 2, international conference, lillafüred, Hungary, 2021
4. M. Sassi, Different methods of the production of foam glass, 2nd ICG-CGCRI Tutorial-completion certificate (silver medal), India, 2021
5. M. Sassi, Glass foam synthesis and properties, the Ceramics and Silicates Conference, Miskolc, Hungary, 2021

Poster Presentation

1. M. Sassi, The chemical durability and stability of foam glass made from soda lime-silicate glass, cathode ray tube glass, and aluminium dross, The 26th International Congress on Glass, Berlin, Germany, 2022

7. Acknowledgement

I would like to take this opportunity to express my sincere gratitude and deep appreciation to my supervisor, Assoc. Prof. Dr. Andrea Simon, for her guidance and patience not only in the academic field but in life too. I get to learn and participate in several events thanks to her. I would like to thank our Solczi Ágnes for being there for me. I think words will not be enough to express gratitude to those two ladies. I would like to express my deepest appreciation to my reviewers and committee especially Dr. Robert Geber for reviewing my report each semester and going patiently through every detail of my reports and giving detailed feedback. I would like to thank Karoly Gal, Filep Ádám for the CT scan, Ildiko Tasnadi, Dr. Roland Szabó for container glass grinding, Dr. Istvan Kocserha for the XRD analysis, Dr. Oliver Banhidi and Ferenc Moricz for the chemical analysis, Dr. Robert Geber for the particle size measurements, Arpad Kovacs for the SEM characterizations, and Prof. Dr. Tamas Kekesi and his team for the cleaning of the dross. I would like to show my respect appreciation and thanks to the glass team at Freiberg University starting with Dr. Fuhrmann Sindy, Stephan, Lena, Magdalina, and Christa Fritzsche for the ICP measurements. I would like to thank Prof. Dr.-Ing. Lothar Wondraczek, the Otto-Schott-Institute University of Jenahe for choosing me in the Glass Future Fellows Program of 2022.

I also wish to thank the Institute of Ceramics and Polymer Engineering and the Antal Kerpely Doctoral School of Materials Science & Technology (Faculty of Materials Science & Engineering) at the University of Miskolc.Thanks to the Stipendium Hungaricum Program, I was able to study at the University of Miskolc.

Bibliography

[1] P. C. Román, J. V. Calvo, A. L. Gil, J. König and M. Á. Rodríguez-Perez, “Modelling of the mechanisms of heat transfer in recycled glass foams,” *Construction and Building Materials,* vol. 274, p. 122000, 2021.

[2] Y. Attila, M. Guden and A. Tasdemirci, "Foam glass processing using a polishing glass powder residue," *Elsevier Ceramics International,* vol. 39, pp. 5869-5877, 2013.

[3] M. Marinov, L. Lakov and Toncheva, "Granulated foam glass. Production, physical and mechanical properties," *SCIENTIFIC PROCEEDINGS XIII INTERNATIONAL CONGRESS "MACHINES. TECHNOLOGIES. MATERIALS,* vol. 10 , no. 12, pp. 42-44, 2016.

[4] N. Karandashova, B. Goltsman and E. Yatsenko, "Analysis of Influence of Foaming Mixture Components on Structure and Properties of Foam Glass," in *IOP Conf. Series: Materials Science and Engineering*, Novocherkassk, 2017.

[5] H. Wang, Z. Chen, R. Ji, L. Liu and X. Wang, "Integrated utilization of high alumina fly ash for synthesis of foam glass ceramic," *Ceramics International,* vol. 44, no. 12, pp. 13681-13688, 2018.

[6] C. Xi, F. Zheng, X. Jiahe, W. Yang, Y. Peng, Y. Li, P. Li and Q. Zhen, "Preparation of glass-ceramic foams using extracted titanium tailing and glass waste as raw materials," *Construction and Building Materials,* vol. 190, p. 896–909, 2018.

[7] R. Lebullenger and F. O. Mear, “Glass recycling,” in *Springer Handbook of Glass*, Springer, 2019, pp. 1355-1377.

[8] Q. Ma, Q. Wang, L. Luo and F. Chaozhen, "Preparation of high strength and low-cost glass ceramic foams," *IOP,* vol. 52, no. 39, 2018.

[9] V. Cosmin and I. Lazău, "Glass foam from window panes and bottle glass wastes," *Central European Journal of Chemistry,* vol. 12, pp. 804-811, 2013.

[10] H. Shi, K.-q. Feng, H.-b. Wang, C.-h. Chen and H.-l. Zhou, "Influence of aluminium nitride as a foaming agent on the preparation of foam," *International Journal of Minerals, Metallurgy and Materials,* vol. 23, no. 5, p. 595, 2016.

[11] R. Ji, Y. Zheng, Z. Zou, Z. Chen, S. Wei, X. Jin and M. Zhang, “Utilization of mineral wool waste and waste glass for synthesis of foam glass at low temperature,” *Construction and Building Materials*, vol. 2015, p. 623–632, 2019.

[12] Z. Chen, H. Wang, R. Ji, L. Liu, C. Cheeseman and X. Wang, "Reuse of mineral wool waste and recycled glass in ceramic foams," *Ceramics International,* vol. 45, p. 15057–15064, 2019.

[13] C. Bai, H. Li, E. Bernardo and P. Colombo, "Waste-to-resource preparation of glass-containing foams from geopolymers," *Ceramics International,* vol. 45, pp. 7196-7202, 2019.

[14] A. Rincon, D. Desideri and E. Bernardo, "Functional glass-ceramic foams from ‘inorganic gel casting’ and sintering of glass/slag mixtures," *Journal of Cleaner Production,* vol. 187, pp. 250-256, 2018.

[15] L. Taoyong, L. Changwei, L. Jianlei, H. Lei, G. Hua, L. Cui, Z. Xin, T. Hui, Y. Qifeng and L. Anxian, “Phase evolution, pore morphology and microstructure of glass ceramic foams derived from tailings wastes,” *Ceramics International,* vol. 44, p. 14393–14400, 2018.

[16] L. Taoyong, L. Changwei, L. Piao, L. Jianlei, L. Cui, H. Lei, X. Zhou, Y. Qifeng and L. Anxian, "Preparation and characterization of partially vitrified ceramic material," *Journal of Non-Crystalline Solids,* vol. 505, p. 92–101, 2019.

[17] L. Taoyong, L. Piao, G. Xiaogang, Z. Jiashuo, H. Qianxing, L. Zhiwei, X. Zhou, Y. Qifeng, T. Yougen and L. Anxian, “Preparation, characterization and discussion of glass ceramic foammaterial: Analysis of glass

phase, fractal dimension and self-foaming mechanism," *Materials Chemistry and Physics,* vol. 243, p. 122614, 2020.

[18] Y. Qi, X. Xiao, Y. Lu, J. Shu, J. Wang and M. Chen, "Cathode ray tubes glass recycling: A review," *Science of The Total Environment,* Vols. Volume 650, Part 2, pp. 2842-2849, 2019.

[19] G. Mucsi, B. CsYke, M. Kertész and L. Hoffmann, "Physical Characteristics and Technology of Glass Foam from Waste Cathode Ray Tube Glass," *Journal of Materials,* vol. 2013, p. 11, 2013.

[20] F. Méar, P. Yot, M. Cambon and M. Ribes, "The characterization of waste cathode-ray tube glass," *Waste Management,* vol. 26, no. 12, pp. 1468-1476, 2006.

[21] S. Pindar and N. Dhawan, "Characterization and recycling potential of the discarded cathode ray tube monitors," *Resources, Conservation and Recycling,* vol. 169, p. 105469, 2021.

[22] Y. Li, Q. Ziyi, L. Chunlei, Q. Yi, W. Haibin, P. Li and W. Yi, "Hazardous characteristics and transformation mechanism in hydrometallurgical disposing strategy of secondary aluminum dross," *Journal of Environmental Chemical Engineering,* vol. 9, no. 6, p. 106470, 2021.

[23] P. Tsakiridis, "Aluminium salt slag characterization and utilization – A review," *Journal of Hazardous Materials,* vol. 217–218, p. 1–10, 2012.

[24] P. Tsakiridis, P. Oustadakis and S. Agatzini-Leonardou, "Aluminium recovery during black dross hydrothermal treatment," *Journal of Environmental Chemical Engineering,* vol. 1, no. 1–2, pp. 23-32, 2013.

[25] A. Kudyba, S. Akhtar, I. Johansen and J. Safarian, "Aluminum recovery from white aluminum dross by a mechanically activated phase separation and remelting process," *The Journal of The Minerals, Metals & Materials Society (TMS),* vol. 73, no. 9, p. 2625–2634, 2021.

[26] M. Sassi and A. Simon, "Waste-to-Reuse Foam Glasses Produced from Soda-Lime-Silicate Glass, Cathode Ray Tube Glass, and Aluminium Dross," *Inorganics,* vol. 10, no. 1, p. 1, 2021.

[27] M. Sassi, J.-E. F. M. Ibrahim and A. Simon, "Characterization of foam glass produced from waste CRT glass and aluminium dross," in *Journal of Physics Conference Series*, Miskolc, 2020.

[28] H. Shen, B. Liu, Z. Shi, S. Zhao, J. Zhang and S. Zhang, "Reduction for heavy metals in pickling sludge with aluminum nitride in secondary aluminum dross by pyrometallurgy, followed by glass ceramics manufacture," *Journal of Hazardous Materials,* vol. 418, p. 126331, 2021.

[29] A. A. El-Amir, M. A. Attia, M. Newishy, T. Fend and M. Emad, "Aluminium dross/soda lime glass waste-derived high-quality glass foam," *Journal of Materials Research and Technology,* vol. 15, pp. 4940-4948, 2021.

[30] M. Mahinroosta and A. Allahverdi, "Hazardous aluminum dross characterization and recycling strategies: Acritical review," *Journal of Environmental Management,* vol. 223, pp. 452-468, 2018.

[31] N. Su, Z. Li, Y. Ding, H. Yang, J. Zhang and G. Fu, "Waste, Waste to Wealth Strategy: Preparation and Properties of Lightweight Al2O3-SiO2-Rich Castables Using Aluminum Dross," *Materials,* vol. 14, no. 24 , p. 7803, 2021.

[32] N. A. Roslan, S. Z. Abidina, O. U. Osazuwa, S. Y. Chin and Y. Taufiq-Yap, *International Journal of Hydrogen Energy,* vol. 46, no. 60, pp. 30959-30975, 2021.

[33] P. Ramaswamy, P. Tilleti, S. Bhattacharjee, R. Pinto and S. A. Gomes, "Synthesis of value added refractories from aluminium dross and zirconia composites," *Materials Today: Proceedings,* vol. 22 part 4, p. 1264–1273, 2020.

[34] E. Elsarrag, A. Elhoweris and Y. Alhorr, "The production of hydrogen as an alternative energy carrier from aluminium waste," *Energy, Sustainability and Society,* vol. 7, p. 9, 2017.

[35] E. David and J. Kopac, “Hydrolysis of aluminum dross material to achieve zero hazardous waste,” *Journal of Hazardous Materials,* vol. 209–210, pp. 501-509, 2012.

[36] P. Liu, L. Liu, Z. Zhou, Y. Li, H. Yuan, Huhetaoli and T. Lei, “Co-pyrolysis of pine sawdust with aluminum dross for immobilization of heavy metal and enhancing hydrogen generation,” *Fuel,* vol. 305, p. 121597, 2021.

[37] A. Meshram, A. Jain, D. Gautam and K. K. Singh, “Synthesis and characterization of tamarugite from aluminium dross: Part I,” *Journal of Environmental Management,* vol. 232, pp. 978-984, 2019.

[38] A. Meshram, R. Jha and S. Varghese, “Towards recycling: Understanding the modern approach to recover waste aluminium dross,” *Materials Today: Proceedings,* vol. 46 Part 3, pp. 1487-1491, 2021.

[39] O. Corning, “FOAMGLAS,” 2020. [Online]. [Accessed 1 May 2022].

[40] y. I. Illés, M. Sassi, H. Zakiyya and T. Kékesi, “Fluoride Salts from Secondary Aluminium DrossThe Fundamental Kinetic Characteristics of Aqueous Dissolution of Chloride and,” in *International Multidisciplinary Scientific Conference* , Miskolc, 2019.

[41] "C-THERM TCi," [Online]. Available: https://ctherm.com/products/tci_thermal_conductivity/how_the_tci_works/mtps/.

[42] J. Zhang, B. Liu, S. Zhao, H. Shen, J. Liu and S. Zhang, “Preparation and characterization of glass ceramic foams based on municipal solid waste incineration ashes using secondary aluminum ash as foaming agent,” *Construction and Building Materials,* vol. 262, p. 120781, 2020.

[43] C. Mavrogonatos, P. Voudouris, J. Berndt, S. Klemme, F. Zaccarini, P. Spry, V. Melfos, A. Tarantola, M. Keith, R. Klemd and K. Haase, “Trace Elements in Magnetite from the Pagoni Rachi Porphyry Prospect, NE Greece: Implications for Ore Genesis and Exploration,” *Minerals,* vol. 725, p. 9, 2019.

[44] K. V. Shailendra, K. D. Vijay and P. D. Shashi, “Utilization of aluminium dross for the development of valuable product – A review,” *Materials Today: Proceedings,* Vols. Volume 43, Part 1, pp. 547-550, 2021.

[45] G. Qin, G. Qiang, L. Yongli, R. Baozeng, F. Mingbo, L. Huilin, T. Dengchao and D. Min, “Innovative technology for defluorination of secondary aluminum dross by alkali leaching,” *Minerals Engineering,* vol. 172, p. 107134, 2021.

[46] A. Tripathy, S. Mahalik, C. .. Sarangi, B. Tripathy, K. Sanjay and I. Bhattacharya, “A pyro-hydrometallurgical process for the recovery of alumina from waste aluminium dross,” *Minerals Engineering,* vol. 137, pp. 181-186, 2019.

[47] Z. Zhengping, L. Han, R. Li, L. Fengqin and Z. Hongliang, “A new approach to recover the valuable elements in black aluminum dross,” *Resources, Conservation and Recycling,* vol. 174, p. 105768, 2021.

[48] H. Lv, M. Xie, L. Shi, H. Zhao, Z. Wu, L. Li, R. Li and F. Liu, “A novel green process for the synthesis of high-whiteness and ultrafine aluminum hydroxide powder from secondary aluminum dross,” *Ceramics International,* vol. 48, no. 1, pp. 953-962, 2022.

[49] H. Shen, B. Liu, C. Ekberg and S. Zhang, “Harmless disposal and resource utilization for secondary aluminium dross: A review,” *Science of The Total Environment,* vol. 760, p. 143968, 2021.

[50] Q. Li, Q. Yang, G. Zhang and Q. Shi, “Investigations on the hydrolysis behavior of AlN in the leaching process of secondary aluminum dross,,” *Hydrometallurgy,* vol. 182, pp. 121-127, 2018.

[51] S. M. El-Haggar, “Sustainability of Municipal Solid Waste Management,” in *Sustainable Industrial Design and Waste Management,* 2007, pp. 149-196.

[52] “Impact of glass from cathode ray tubes (CRT) in achieving the WEEE recycling and recovery targets,” WEEE Forum, 2018.

[53] J. König, A. Lopez-Gil, P. Cimavilla-Roman, M. A. Rodriguez-Perez, R. R. Petersen, M. B. Østergaard, N. Iversen, Y. Yue and ˇ. S. Matjaz, "Synthesis and properties of open- and closed-porous foamed glass with a low density," *Construction and Building Materials,* vol. 247, p. 118574, 2020.

[54] S. S. Owoeye, G. O. Matthew, F. O. Ovienmhanda and S. O. Tunmilayo, "Preparation and characterization of foam glass from waste container glasses and water glass for application in thermal insulations," *Ceramics International,* vol. 46, no. 8, p. 11770–11775, 2020.

[55] M. B. Østergaard, M. Zhang, X. Shen, R. R. Petersen, J. König, P. D. Lee, Y. Yue and B. Cai, "High-speed synchrotron X-ray imaging of glass foaming and thermal conductivity simulation," *Acta Materialia,* vol. 189, pp. 85-92, 2020.

[56] A. H. A., M. S. Mohammed, M. A. Arif and H. Shoukry, "Reuse of lead glass sludge in the fabrication of thermally insulating foamed glass with outstanding properties and high Pb-stabilization," *Environmental Science and Pollution Research,* vol. 29, p. 47209–47224, 2022.

[57] M. Davraz, ·. K. M., A. A. E., Ş. Kılınçarslan, Y. E. Delikanlı and M. Çabuk, "An investigation of foaming additives and usage rates in the production of ultra-light foam glass," *Journal of Thermal Analysis and Calorimetry,* vol. 147, p. 3567–3576, 2022.

[58] J. König, V. Nemanic, M. Zumer, R. R. Petersen, M. B. Østergaard, Y. Yue and D. Suvorov, "Evaluation of the contributions to the effective thermal conductivity of an open-porous-type foamed glass," *Construction and Building Materials,* vol. 214, p. 337–343, 2019.

[59] H. Zhao and C.-S. Poon, "Recycle of large amount cathode ray tube funnel glass sand to mortar with supplementary cementitious materials," *Construction and Building Materials,* vol. 308, p. 124953, 2021.

[60] R. C. da Silvaa, E. T. Kubaski, E. T. Tenório-Neto, M. K. Lima-Tenório and S. M. Tebcherani, "Foam glass using sodium hydroxide as foaming agent: Study on the reaction mechanism in soda-lime glass matrix," *Journal of Non-Crystalline Solids,* vol. 511, p. 177–182, 2019.

[61] M. B. Østergaard, M. Zhang, X. Shen, R. R. Petersen, J. Konig, P. D. Lee, Y. Yue and B. Cai, "High-speed synchrotron X-ray imaging of glass foaming and thermal conductivity simulation," *Acta Materialia,* vol. 189, pp. 85-92, 2020.

[62] B. D. Zdravkov, J. J. Cermak, M. Sefara and J. Janku, "Pore classification in the characterization of porous materials: A perspective," *Central european journal of chemistry,* vol. 5, no. 2, p. 385–395, 2007.